Applied Catalysis B: Environmental 339 (2023) 123129

Contents lists available at ScienceDirect

Applied Catalysis B: Environmental

journal homepage: www.elsevier.com/locate/apcatb

Waste to wealth: H_2S-free fabrication of Fe-ZnS/NC by industrial lignin self S-doping for efficient lignin aerobic oxidation

Haiwei Guo [a,*], Zhao Chen [a], Qiqi Yin [a], Tian Sun [a], Yuxuan Liu [b], Gengbo Ren [a], Changzhi Li [c,*]

[a] School of Energy and Environmental Engineering, Hebei University of Technology, Tianjin 300401, China
[b] Shaanxi Key Laboratory of Low Metamorphic Coal Clean Utilization, School of Chemistry and Chemical Engineering, Yulin University, Yulin 719000, China
[c] CAS Key Laboratory of Science and Technology on Applied Catalysis, Dalian Institute of Chemical Physics, Chinese Academy of Sciences, Dalian 116023, China

ARTICLE INFO

Keywords:
H_2S-free
Fe-Zn bimetallic sulfide
Industrial lignin
Self S-doping
Lignin oxidation

ABSTRACT

Industrial lignin mostly contains sulfur, which poisons metal catalysts easily. Metal sulfides with good S-resistance could be used as efficient catalysts for lignin oxidation, while metal sulfides preparation involved corrosive H_2S. Here in, we proposed H_2S-free fabrication of bimetallic Fe-ZnS/NC by industrial lignin self S-doping. The Fe-ZnS/NC 650 exhibited efficient oxidation activity (> 99% conversion) for β-O-4 cleavage and good S-resistance for industrial lignin oxidation. Density functional theory revealed the synergistic effect of FeS and ZnS in lignin oxidation, where FeS tended to activate O_2 into superoxide radical ($O_2^{\bullet-}$) and ZnS contributed to the polarization of β-O-4. The dual sites greatly reduced the migration distance of $O_2^{\bullet-}$ to the polarized β-O-4, facilitating the C-O/C-C cleavage. Hence, Fe-ZnS/NC 650 selectively converted lignin into carbonyl-containing aromatics with up to 92% selectivity under alkaline-free condition. This work developed a novel strategy using lignin-derived metal sulfide without external sulfur source for efficient lignin degradation.

1. Introduction

Lignin, the most abundant aromatic components in the nature, has been considered as a promising substitute for fossil resource in view of renewability and carbon neutrality [1–6]. Hydrogenolysis and oxidation are two commonly used approaches for lignin valorization, among which oxidative depolymerization has been considered as a potential strategy to achieve oxygen-functional enriched platform compounds (e.g., acid, aldehyde, phenol) under mild condition when comparing with hydrogenolysis that generally required harsh condition such as high temperatures or high hydrogen pressures [7–9]. However, additional acid or base was always required under most of the current catalytic system for lignin oxidative depolymerization [10,11]. Moreover, industrial lignin wastes (such as lignosulfonate and alkaline lignin from papermaking waste liquor) contained sulfur which coordinate easily with most of metal, leading to rapid deactivation of metal-based catalysts [12]. Therefore, we attempted to develop a highly efficient catalyst with excellent sulfur-resistance and oxidation activity for lignin aerobic polymerization under non-acid/base conditions.

Metal sulfides have shown superior oxidation activity in degrading organic pollutants and have been widely applied to electrocatalysis/photocatalysis area [13]. For example, Wu et al. reported that the developed CoS@FeS electrocatalytic material could accelerate the activation of peroxymonosulfate (PMS) into hydroxyl radical, achieving 99.1% oxidative removal of sulfamethoxazole [13]. Rashi and co-workers synthesized ZnS supported MoS nanosheet and it achieved 81% oxidative degradation of oxytetracycin under visible light irradiation [14]. Metal sulfide materials have been also investigated for lignin degradation by the electrocatalytic/photocatalytic strategy [15]. For instance, Fang and co-workers synthesized dodecyl sulfate-intercalated CoS nanocones, and it could electrolytically depolymerize lignin to aryl aldehydes (21.4 wt%) or carboxylic acids (23.9 wt%) [16]. Ni-modified CdS nanosheet photocatalytic materials developed by Han et al. decomposed lignin models into aromatic products at room temperature [17]. Similarly, the $Zn_4In_2S_7$ synthesized by Lin and co-workers effectively cleaved C-O bond in β-O-4 under visible light irradiation [15]. Upon the above progresses of metal sulfides in lignin oxidation by electrocatalytic or photocatalytic method, we're eager to know that whether metal sulfides could be feasible for the thermo-catalytical lignin oxidation, especially seldom related study has been conducted so far.

The key to developing efficient metal sulfide catalysts for lignin aerobic oxidation lies on constructing the active sites for O_2 activation and C-O/C-C cleavage. Recently, Zhang and co-worker reported that enzyme-mimic Fe-based catalyst with FeN_3 motifs could active O_2 into

* Corresponding authors.
E-mail addresses: guohaiwei@hebut.edu.cn (H. Guo), licz@dicp.ac.cn (C. Li).

https://doi.org/10.1016/j.apcatb.2023.123129
Received 2 June 2023; Received in revised form 10 July 2023; Accepted 24 July 2023
Available online 25 July 2023

superoxide radical, which hence favor C-C cleavage in aromatic ketones at room temperature [18]. Zn-based catalysts also demonstrated as efficient catalysts for the oxidative cleavage of C(CO)-C bonds in acetophenone into esters by superoxide radical from O_2 activation [19]. We hence assumed that it's possible to develop Fe or Zn-based sulfide for lignin oxidative depolymerization. However, in radical predominant aerobic reactions, the half-life periods of most reactive oxygen-containing radicals are quite short, and the solutions to reduce the migration path of reactive radicals to target organic molecules are highly desired to maximize the catalytic performance [20]. Bimetallic systems were generally considered to possess superior catalytic performance due to the synergistic effects between two metal sites [21], e.g., a recently reported Fe-ZnS quantum dots with dual-reaction centers showed prominent catalytic activity in activating dissolved O_2 to $^1O_2$ and the followed fast oxidative degradation of bisphenol A (BPA), with 97.2% removal rate of BPA in only 15 s [22]. Therefore, it's possible to synthesize bimetallic Fe-Zn sulfide to boost the oxidation activity of metal sulfide for lignin depolymerization.

Currently, most of the strategies for metal sulfides synthesis used thiourea, thiopropionamide or sodium sulfide as sulfur precursor, and the decomposition of which would involve the formation of highly corrosive H_2S gas, which seriously threatened the environment or equipment [23–25]. Taking advantage of the sulfur-containing feature of industrial lignin waste, it's possible to fabricate H_2S-free Fe-Zn sulfide catalyst by industrial lignin self S-doping for lignin valorization. Besides, it's reported that lignin can coordinate with transition metal ions and favor the dispersion of metal atoms [26,27], and using industrial lignin wastes as eco-friendly substitutes of carbon and sulfur precursor is highly feasible to synthesize well dispersed Fe-Zn sulfide. Currently, the utilization of bimetallic Fe-Zn sulfide for lignin oxidation hasn't been investigated, and it's highly required to determine the accurate active sites on the bimetallic sulfide catalysts for O_2 activation and C-O/C-C cleavage.

Here in, we synthesized H_2S-free self S-doped bimetallic Fe-ZnS/NC using waste industrial lignin, and the as-prepared bimetallic Fe-ZnS/NC-650 exhibited excellent aerobic oxidation activity for β-O-4 depolymerization under non-alkaline/acid conditions. Especially, our adopted oxidation-oxidation strategy provided 92% selectivity of carbonyl-containing aromatics based on 11.81 wt% yield of total detected monomers under alkaline-free condition, while the previous reported oxidation-hydrogenolysis strategy mostly provided varied aromatic monomers with different linkages (Scheme 1). Furthermore, density functional theory (DFT) calculation was used to illustrate the synergistic function of Fe-Zn dual-sites for O_2 activation and C-O/C-C cleavage. Finally, the reaction mechanism for lignin oxidative depolymerization over Fe-ZnS/NC-650 was proposed.

2. Experimental section

2.1. Synthesis of the as-prepared catalysts

To synthesize Fe-ZnS/NC, 2 g industrial alkaline lignin was firstly dissolved in 150 mL deionized water with stirring. Meanwhile, 2.7209 g (10 mmol) ferric chloride hexahydrate and 2.195 g (10 mmol) zinc acetate were firstly dissolved in 50 mL deionized water, which was then added into lignin solution. After stirring for 1 h, the formed Fe/Zn-lignin complex was aged for 10 h followed by drying the obtained complex at 60 °C for 36 h. Thereafter, a certain amount of dicyandiamide was mixed with the above dried solids, which was pre-pyrolyzed at 550 °C for 1 h and then at 550/650/800 °C for another 1 h under N_2 atmosphere (heating rate: 5 °C/min, flow rate: 150 mL/min). After cooling, the resulting catalyst was washed by 100 mL 1 mol/L HCl solution for 4 h followed by deionized water until the filtrate became neutral. After dried at 80 °C for 2 h, the obtained materials were named Fe-ZnS/NC 550/650/800. Fe-Zn/NC 650 was prepared using S-free corn straw instead of industrial alkaline lignin as carbon precursor under identical conditions as Fe-ZnS/NC 650. ZnS/NC 650 (or FeS/NC 650) was prepared at 650 °C as above procedures except that no ferric chloride hexahydrate (or zinc acetate) was added. NC 650 catalyst was prepared at 650 °C by mixing 2.0 g of lignin with 1.0 g of dicyandiamide without adding either ferric chloride hexahydrate or zinc acetate.

2.2. Characterizations of the prepared catalysts

X-ray diffraction (XRD) analysis was proceeded on a Rigaku SmartLab SE using Cu Kα radiation with a scanning angle (2θ) of 5° to 90°, operated at 40 kV and 40 mA. X-ray photoelectron spectroscopy (XPS) was measured on a Thermofisher escalab 250xi. High-resolution transmission electron microscopy (HRTEM) and energy-dispersive X-ray spectroscopy (EDX) mappings were recorded on a JEM-F200 (HRP) electron microscope. The N_2 adsorption−desorption measurement was conducted on ASAP 2460 instrument and the samples were degassed at 120 °C. Raman spectra of the powder samples were recorded by LabRAM HR Evolution Raman spectrometer at 532 nm. The metal loading on the catalyst was measured using Inductively Coupled Plasma Atomic Emission Spectroscopy (ICP-AES) on a Thermo Fisher iCAP PRO

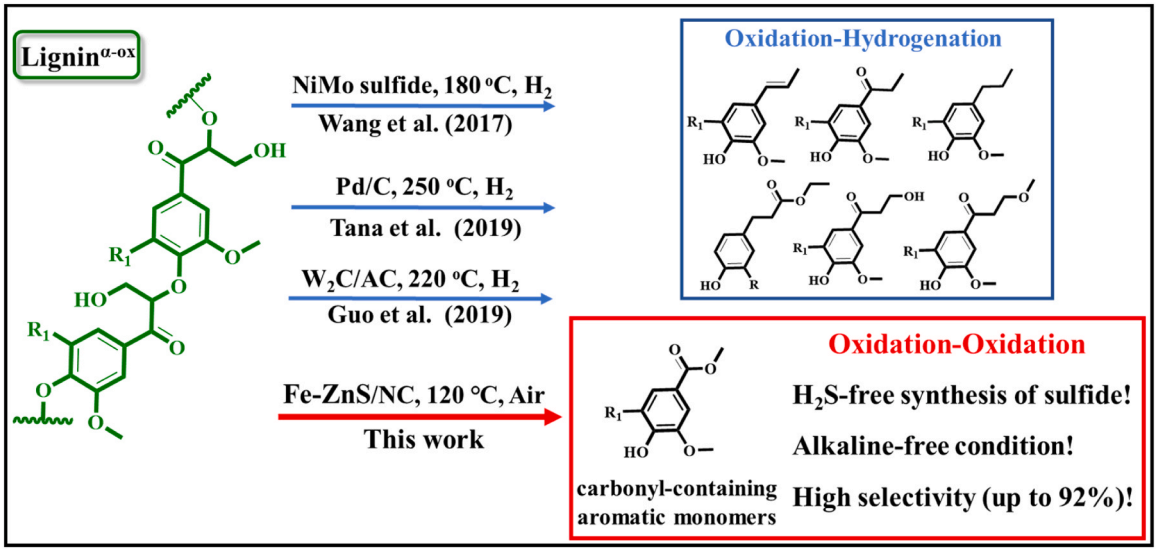

Scheme 1. Previously reported oxidation-hydrogenation strategies [28–30] and the developed oxidation-oxidation method in this work.

instrument. EPR spectroscopy was performed on a Bruker EMX PLUS at the X-band at 100 °C with a field modulation of 100 kHz. In detail, 10 mg Fe-ZnS/NC 650 or NC 650 with 5 mL methanol were mixed in a beaker, heating to 100 °C in water bath and filling with O_2 for 10 min. After the reaction, the spin-trapping reagent DMPO was added to the reaction mixture which was measured in a glass capillary tube by EPR spectroscopy. 2D HSQC NMR was performed on a Bruker AVAVCE III HD 700 MHz spectrometer at 25 °C with 50 mg lignin or liquid oil in 0.6 mL d_6-DMSO.

2.3. Catalytic oxidative cleavage of β-O-4 model compounds

The reaction was carried out in a stainless autoclave (50 mL). In detail, 20 mg model compound, 20 mg catalyst, and 20 mL methanol were put into the autoclave. The reactor was filled with 1 MPa air after flushing by N_2 for three times and then reacted 2 h at 120 °C. GC 9720 PLUS instrument (FULI INSTRUMENTS) was used to for quantification of the products. GC-MS (Varian 450 GC-320 MS) was used to identify the products according to the NIST library 2020.

SCN^- poisoning reaction: 50 mg Fe-ZnS/NC 650 catalyst was put into 100 mL NaSCN solution (4 mg/mL) with stirring for 4 h. After reaction, the resulting catalyst was washed with deionized water and ethanol repeatedly. The SCN^- treated catalyst was then applied to β-O-4 oxidation under the same condition unless otherwise specified. S poisoning reaction: Fe-ZnS/NC 650 or Ru-NC was put into a tubular furnace and treated by 4.98% SO_2 standard gas (2 mL/min) at 120 °C for 2 h, After reaction, the resulting catalyst was washed with deionized water and ethanol repeatedly. The S-treated catalyst was then applied to β-O-4 oxidation under identical condition.

2.4. Catalytic oxidative depolymerization of beech lignin

The oxidative depolymerization of beech lignin was conducted as following: 100 mg oxidized beech lignin (labelled as $lignin^{OX}$) which was obtained by the stoichiometric oxidation using 1.33 wt% equiv. DDQ (2,3-dichloro-5,6-dicyano-1,4-benzoquinone) according to our previous report [31], 50 mg catalyst, and 20 mL of methanol were added into the autoclave with stirring. The reactor was filled with 1 MPa air after flushing by N_2 for three times and was then conducted at 200 °C for 2–10 h. After reaction, the filtrate was concentrated under reduced pressure at 35 °C to obtain the liquid oil which was then diluted by 1 mL with methanol with mesitylene as the internal standard. Internal standard method was adopted for products quantification and the retention time of all the detected products and standard curves were shown in supporting information.

3. Results and Discussion

3.1. Characterization and activity evaluation of as-prepared Fe-ZnS/NC

Fig. 1**A** showed the HRTEM and EDX images of the prepared Fe-ZnS/NC 650. The observation of the lattice spacing with 0.31 nm attributing to ZnS (111) crystal plane (PDF #77–2100) and that of 0.26 nm to FeS (200) crystal plane (PDF #89–4076) suggested the co-existence of FeS and ZnS in Fe-ZnS/NC 650. Besides, EDX demonstrated the successful introduction of S, Zn, Fe in Fe-ZnS/NC 650. The existence of ZnS was in Fe-ZnS/NC 650 also confirmed by the XRD results in Fig. S1A, where three diffraction peaks at 28.6°, 48.1°, and 56.8° attributing to the (111), (220), and (311) crystal planes in sphalerite structure ZnS (PDF #77–2100) were detected. XPS spectra also confirmed the existence of Fe, Zn, and S elements with atomic contents of 0.91%, 2.40%, and 2.41%, respectively (Table S1). More importantly, as shown in Fig. 1**B**, Fe-ZnS/NC 650 possessed relatively higher content of S^{2-} from ZnS or FeS at 161.4–163.0 eV [22,32] than that of FeS/NC and ZnS/NC which showed either relative higher amount of sulfate at 168.3 eV [33] or S-C at 164.6 eV [34]. It should note that it's difficult to distinguish ZnS or FeS solely by XPS due to their similar binding energy position [35,36], while the co-existence of FeS and ZnS has been confirmed by the HRTEM results in Fig. 1**A**.

2-Phenoxy-1-phenylethanone labelled as β-O-4 (1), a common dimeric model compound of oxidized lignin, was initially selected in this work. As shown in Table 1, β-O-4 (1) could be converted to phenol (**a**),

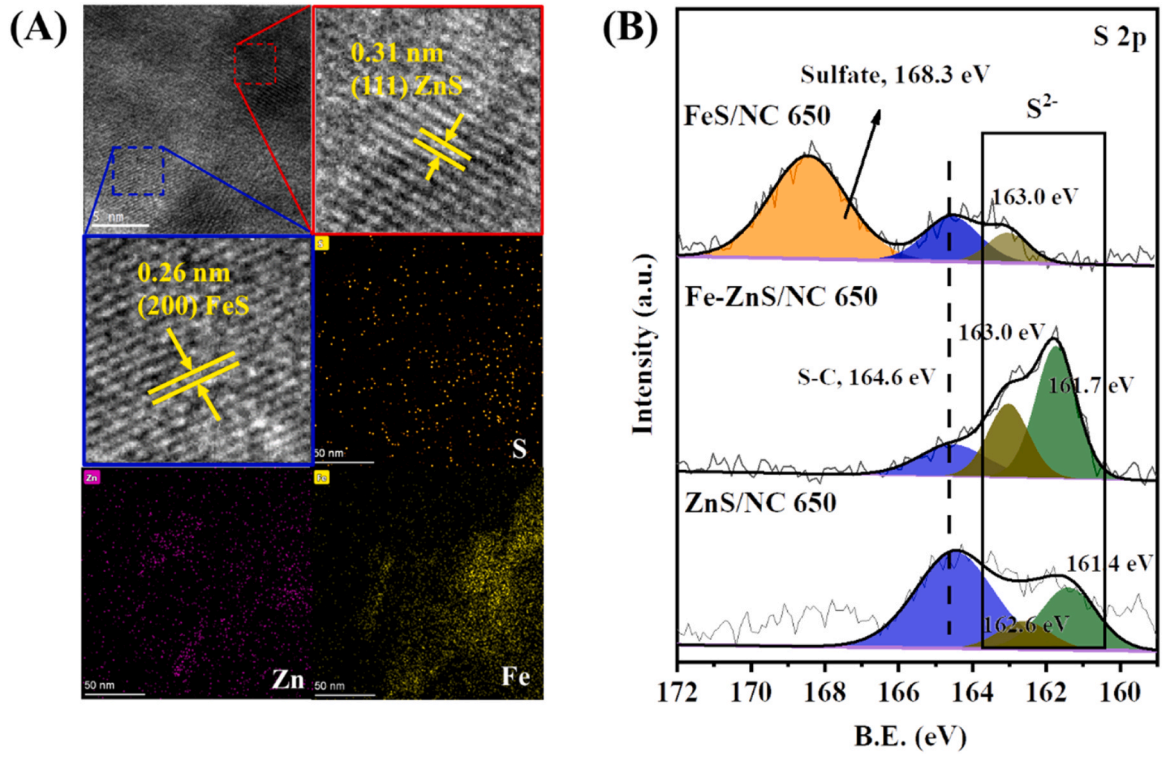

Fig. 1. **(A)** HRTEM and EDX mapping of Fe-ZnS/NC 650; **(B)** S 2p spectra of FeS/NC 650, ZnS/NC 650 and Fe-ZnS/NC 650.

Table 1
The catalytic oxidative cleavage of β-O-4 model compound (2-Phenoxy-1-phenylethanone) under various conditions.

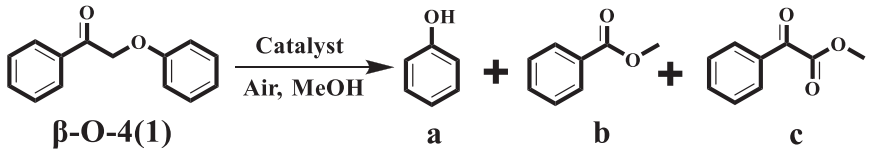

Entry	Catalyst	Conv. (%)	Yield (%)		
			a	**b**	**c**
1	-	< 1.0	-	-	-
2	NC 650	31.1	25.3	19.0	
3	Fe-ZnS/NC 650	99.0	88.2	66.6	15.8
4[a]	Fe-ZnS/NC 650	44.0	41.7	16.0	-
5	ZnS/NC 650	60.8	54.1	38.0	10.3
6	FeS/NC 650	63.8	58.2	39.1	10.6
7[b]	ZnS/NC 650 + FeS/NC 650	61.8	52.1	36.8	9.3
8	Fe-Zn/NC 650	88.7	50.0	36.4	15.6
9	Fe-ZnS/NC 550	76.6	73.3	36.0	10.6
10	Fe-ZnS/NC 800	52.5	46.4	22.1	6.3
11[c]	Fe-ZnS/NC 650	74.7	73.5	48.1	7.5
12[d]	Fe-ZnS/NC 650	88.7	83.9	51.1	10.7
13[e]	Fe-ZnS/NC 650	99.0	90.5	65.8	16.0
14[f]	Fe-ZnS/NC 650	29.5	21.9	-	-
15[g]	Fe-ZnS/NC 650	48.2	40.1	-	-
16[h]	Fe-ZnS/NC 650	34.9	34.9	-	-

Reaction conditions: substrate (20 mg), catalyst (20 mg), methanol (20 mL), air (1 MPa), 120 °C, 2 h.
a: 1 MPa N_2.
b: Physical mixture with mass ratio of 1:1.
c: 80 °C, 2 h.
d: 100 °C, 2 h.
e: 120 °C, 4 h.
f: acetonitrile.
g: ethanol.
h: acetone.

methyl benzoate (**b**), and methyl benzoylformate (**c**) over our catalytic system. When no catalyst was added (entry 1), less than 1% of β-O-4 (1) was converted without any cleavage product detected, indicating that only thermal effect at 120 °C was inefficient for β-O-4 (1) conversion. NC 650 showed 31.1% of β-O-4 (1) conversion and 25.3% yield of phenol (**a**) and 19.0% of methyl benzoate (**b**) (entry 2). Remarkably, with the introduction of Fe and Zn, Fe-ZnS/NC 650 demonstrated sharply increased β-O-4 (1) conversion (99.0%), along with 88.2% yield of phenol (**a**), 66.6% of methyl benzoate (**b**) and 15.8% of methyl benzoylformate (**c**) (entry 3). The above results implied that the introduction of Fe/Zn significantly improved the cleavage efficiency of the C-O/C-C in β-O-4 in comparison with solely NC 650. The good oxidation activity of Fe-ZnS/NC 650 was also confirmed by kinetics study, where Fe-ZnS/NC 650 showed lower activation energy of 64.04 kJ/mol than that of 70.48 kJ/mol for ZnS/NC 650 (Fig. S2). O_2 was proved to be necessary for β-O-4 oxidative cleavage in our Fe-ZnS/NC 650 catalytic system. As shown in Table 1 (entry 4), the conversion of β-O-4 (1) reduced to 44.0% when under pure N_2, with the yields of **a** dropping to 41.7% and **b** to 16.0%, suggesting that O_2 was highly required for β-O-4 oxidative cleavage over Fe-ZnS/NC 650.

To explore the main active sites on Fe-ZnS/NC 650, we performed a series of control experiments for β-O-4 depolymerization. As shown in Table 1 (entry 5), ZnS/NC 650 only gave 60.8% of β-O-4 (1) conversion with low yields of **a** (54.1%), **b** (38.0%), **c** (10.3%) in the absence of Fe. Similarly, only 63.8% conversion of β-O-4 (1) with the yields of **a** (58.2%), **b** (39.1%), **c** (10.6%) was obtained over FeS/NC 650 without Zn (entry 6, Table 1). Besides, the physical mixture of FeS/NC 650 + ZnS/NC 650 also afforded poor β-O-4 (1) conversion (61.8%) and low yields of **a** (52.1%), **b** (36.8%), **c** (9.3%) (entry 7, Table 1). The above phenomenon demonstrated the synergistic effect of coexisted FeS and ZnS on Fe-ZnS/NC 650 that promoted the oxidative cleavage of C-O/C-C in β-O-4 (1) easier. The synergistic effect between FeS and ZnS was also ensured by analysing their chemical valence change by XPS. As shown in Fig. S3 **A&B,** Fe lost electron in Fe-ZnS/NC 650 with the relatively higher binding energy of 711.9 eV than the 711.3 eV in FeS/NC 650 [32]; meanwhile, Zn gained electron in Fe-ZnS/NC 650 with relatively lower binding energy (1022.0 eV) than ZnS/NC 650 (1022.2 eV) [35]. Charge density was further carried out to demonstrate their synergistic effect in Fig. S3 **C&D**. The charge density of ZnS was observed strengthened (blue colour) whilst the charge density of FeS weakened (yellow colour) on both bare Fe-ZnS/NC 650 and the Fe-ZnS/NC 650 after β-O-4 adsorption, implying that electron was transferred from FeS to ZnS. The above information ensured the synergistic effect between FeS and ZnS. To further prove the function of metal sulfide, sulfide-free Fe-Zn/NC 650 was also prepared using corn straw as carbon precursor without sulfur element (Table S3) instead of using industrial lignin (entry 8), and it provided lower β-O-4 (1) conversion (88.7%) and significantly worse yields of **a** (50.0%), **b** (36.4%) and **c** (15.6%). The above results ensured the importance of Fe-Zn sulfide for C-O/C-C oxidative cleavage in β-O-4 (1).

Previous reports have shown that Fe-N_X or Zn-N_X sites were also effective in O_2 activation and C-O/C-C cleavage [18,19]. To exclude the possible role of Fe-N_X or Zn-N_X sites in β-O-4 oxidative cleavage, NaSCN was added to poison the M-N_X sites on Fe-ZnS/NC 650. As shown in Fig. 2**A**, no significant difference of β-O-4 (1) conversion or monomer yields between the normal or SCN^- poisoned Fe-ZnS/NC 650 was observed, implying the negligible contribution of Fe-N_X or Zn-N_X on β-O-4 (1) depolymerization. Furthermore, when the reaction time was reduced to seconds to control the reaction within kinetically region (Fig. 2**B**), similar results have been obtained with 22.2% conversion of β-O-4 (1) on Fe-ZnS/NC 650 without SCN^-, which was comparable to the value of 20.1% on SCN^- poisoned Fe-ZnS/NC 650. The above results indicated that either Fe-N_X or Zn-N_X but the Fe-ZnS dual sites served as the key active species that boosted the C-O/C-C oxidative cleavage in

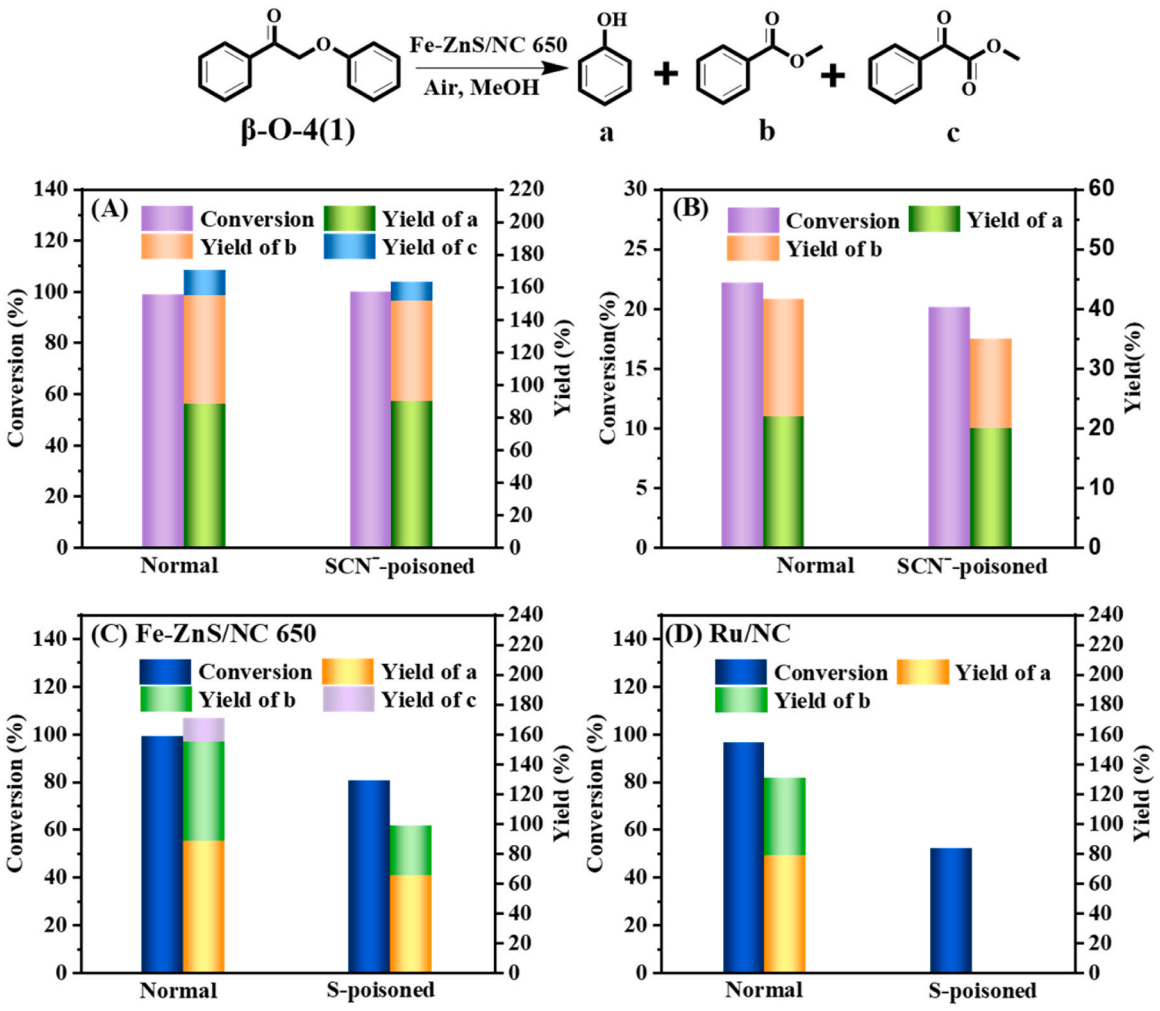

Fig. 2. β-O-4 (1) conversion over normal or SCN^- poisoned Fe-ZnS/NC 650 **(A)** for 2 h and **(B)** for seconds (stop the reaction immediately when the temperature rose to 120 °C). β-O-4 (1) conversion over **(C)** normal and S-poisoned Fe-ZnS/NC 650 and **(D)** normal and S-poisoned Ru-NC for 2 h. Reaction conditions: catalyst (20 mg), methanol (20 mL), 1 MPa air, 120 °C.

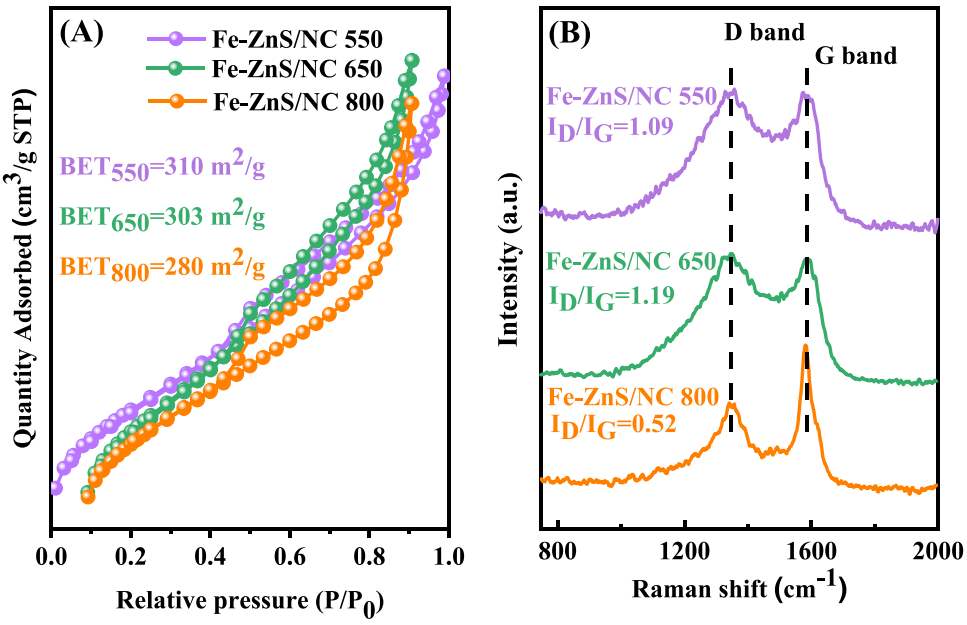

Fig. 3. **(A)** N_2 adsorption—desorption isotherm and **(B)** Raman shift of Fe-ZnS/NC 550, Fe-ZnS/NC 650, Fe-ZnS/NC 800.

β-O-4. Moreover, the good S-resistance of Fe-ZnS/NC 650 was proved through comparing the oxidation activity of normal or S-poisoned Fe-ZnS/NC 650 by SO_2. As shown in Fig. 2**C**, slight decrease of β-O-4 (1) conversion and **a/b/c** yields were observed between the S-poisoned Fe-ZnS/NC 650 and the normal one. By contrast, dramatic reduce of β-O-4 (1) conversion with none of **a/b/c** were observed when using S-poisoned noble metal Ru-NC catalyst (Fig. 2**D**). Fe-ZnS/NC 650 was also feasible to the oxidative depolymerization of sulfur-containing industrial lignin such as lignosulfonate and alkaline lignin (Fig. S4). The above results suggested the superior S-resistance of Fe-ZnS/NC 650.

The catalytic activity of Fe-ZnS/NC prepared at different pyrolysis temperatures (550 °C or 800 °C) was also evaluated (entry 9–10, Table 1). Fe-ZnS/NC 550 achieved relatively lower β-O-4 (1) conversion (76.6%) and yields of **a** (73.3%)**, b** (36.0%) and **c** (10.6%). When the pyrolysis temperature increased to 800 °C, even lower conversion (52.5%) and yields of **a, b** and **c** (46.4%, 22.1% and 6.3%, respectively) were observed on Fe-ZnS/NC 800. The relatively lower catalytic activity of Fe-ZnS/NC 550 could be explained by the absence of sphalerite ZnS confirmed by XRD pattern (Fig. S1A), and the even lower catalytic activity of Fe-ZnS/NC 800 could be resulted from both the lower BET surface area (280 m^2/g, Fig. 3**A**) comparing with Fe-ZnS/NC 650 (303 m^2/g, Fig. 3**A**) and Fe-ZnS/NC 550 (310 m^2/g, Fig. 3**A**) and the less amount of ZnS (as Zn would evaporate at higher temperature). It should note that the good catalytic activity of Fe-ZnS/NC 650 was benefited from balanced amount of ZnS as the β-O-4 conversion and monomer yields decreased either lowering down or increasing the amount of ZnS (Table S2). The pore size distribution demonstrated that pore size showed less effect on the catalytic activity as the three catalysts all showed mesoporous characteristic with the average pore size centered at 4.44–4.68 nm as shown in Fig. S1B. Moreover, Raman analysis showed that Fe-ZnS/NC 650 possessed more surface defects with the highest I_D/I_G = 1.19 when comparing with Fe-ZnS/NC 550 with I_D/I_G = 1.09 and Fe-ZnS/NC-800 with I_D/I_G = 0.52 (Fig. 3**B**). The enriched surface defects could enable enough exposed and accessible active sites on Fe-ZnS/NC 650, thus kinetically favoring O_2 activation [37]. The catalytic activity of Fe-ZnS/NC 650 under different reaction conditions was also conducted (entry 11–16, Table 1). It demonstrated that neither lowering down the reaction temperature (80 °C or 100 °C, entry 11–12) nor replacing methanol by ethanol, acetonitrile or acetone (entry 14–16, Table 1) could notably decrease the β-O-4 (1) conversion and product yields. Meanwhile, no significant increase of β-O-4 (1) conversion and the product yields was observed at longer reaction time (4 h, entry 13, Table 1), indicating that the catalytic reaction at 120 °C in methanol for 2 h was the most appropriate conditions for β-O-4 oxidative depolymerization.

The good catalytic performance of Fe-ZnS/NC 650 was also verified on other β-O-4 model compounds with methoxy group in R_1, R_2, or R_3 position. As shown in Table 2, it showed that the methoxy-substituted β-O-4 substrates were almost fully transformed under Fe-ZnS/NC 650 with phenol derivative (**1**) and methyl benzoate derivatives (**2 & 3**) were the main products, suggesting that the aryl C-O/C-C bonds could be cleaved in our Fe-ZnS/NC 650/methanol/air system. However, the yields of the cleavage products varied for the β-O-4 with the methoxy group at different position. For instance, the yields of the phenol derivatives (**1**) decreased when the methoxyl groups at R_2 or R_3, which varied from 15.3% to 44.9% for β-O-4 (2, 5) & β-O-4 (3, 6) compared with that of 88.2% in β-O-4 (1) and 94.5% in β-O-4 (4) with the methoxyl groups at R_1. Especially, the yields of phenol derivatives (**1**) decreased with the increased number of methoxyl groups. In detail, the yield of phenol derivatives (**1**) decreased from 44.9% in β-O-4 (2) with one methoxyl group to 22.5% in β-O-4 (3) with two methoxyl groups, and the value further reduced to 15.3% in β-O-4 (6) with three methoxyl groups, and the combination of stereochemical and electronic led to above phenomenon [38]. The relatively low mass balance based on the aromatic products was due to the formation of benzoquinone from product over-oxidation (Fig. S5A) or ring-opening products [39,40] which have been observed during the oxidative depolymerization of beech lignin (Fig. S5B).

Table 2
Catalytic oxidative cleavage of various β-O-4 model compounds over Fe-ZnS/NC 650.

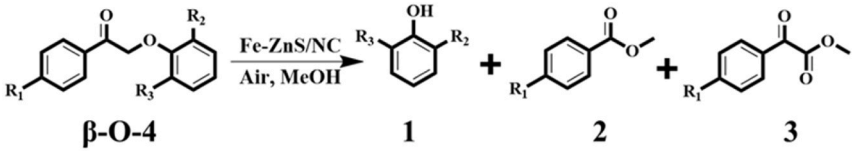

Label	Structure	Conv. (%)	Product distribution (%)		
			1	**2**	**3**
β-O-4 (2)	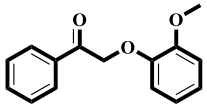	98.3	44.9	59.5	16.0
β-O-4 (3)	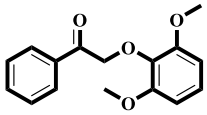	99.0	22.5	63.6	12.6
β-O-4 (4)	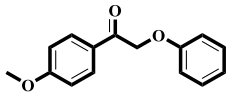	99.0	94.5	44.2	9.3
β-O-4 (5)	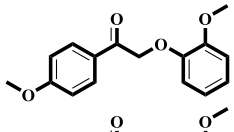	95.9	29.4	58.4	8.8
β-O-4 (6)	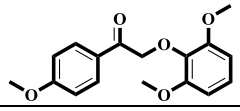	99.0	15.3	72.8	4.5

Reaction conditions: substrate (20 mg), catalyst (20 mg), methanol (20 mL), air (1 MPa), 140 °C, 8 h.

3.2. Exploration for O_2 activation sites on Fe-ZnS/NC 650

O 1 s spectra was firstly used to analyze the oxygen species on Fe-ZnS/NC 650, and three peaks with the binding energies at 533.4 eV assigning to C-OH or C-O-OH group, 531.7 eV to C═O groups, and 529.9 eV to absorbed O_2 were observed in Fig. 4**A** [18]. The existence of peaks at 529.9 eV on Fe-ZnS/NC 650 suggested its strong ability to adsorb O_2 at room temperature [18,19,41]. To probe the truly active species for O_2 activation in our catalytic system, we computed the O_2 activation process on FeS or ZnS by DFT calculation. Fig. 4**B** displayed a model of O_2 adsorbed on Fe-ZnS/NC 650. The bond length of O═O was stretched from 1.209 Å to 1.480 Å at both FeS and ZnS sites (Table S4), indicating that the O═O was affected by Fe-ZnS/NC 650. However, the adsorption energies of O_2 on FeS and ZnS varied, i.e., FeS possessed strong O_2 adsorption ability with the adsorption energy of − 2.661 eV comparing with ZnS sites of − 2.402 eV, implying that O_2 tended to adsorb on FeS sites. It should note that the adsorption energy of β-O-4 (1) on Fe-ZnS/NC (−1.423 eV on FeS sites and −1.744 eV on ZnS sites, Fig. 6**B**) was much higher than that of O_2, indicating that O_2 adsorption should be the initial step in the reaction.

To probe the active radicals produced during the β-O-4 oxidation on Fe-ZnS/NC 650, radical quenching experiments were performed. Firstly, isopropanol, a commonly used quencher to •OH was added in the reaction. As shown in Table 3, the conversion of β-O-4 (1) did not change with the addition of 4 equiv. isopropanol, suggesting that •OH didn't show much influence on β-O-4 (1) oxidation. Similar results were obtained when adding 4 equiv. furfuryl alcohol (a quenching agent to singlet oxygen $^1O_2$) to the reaction system, where only slightly decrease of β-O-4 (1) conversion (from 99.0% to 92.9%) was observed. However, when 4 equiv. 1,4-benzoquinone was added to the reaction as a radical quencher of $O_2^{\bullet-}$, the conversion of β-O-4 (1) significantly reduced to 7.0%. These results suggested that $O_2^{\bullet-}$ radicals played an important role in β-O-4 (1) oxidative cleavage. Furthermore, electron paramagnetic resonance (EPR) measurements were performed to verify the reactive oxygen species involved in the reaction using 5,5-dimethyl-1-pyrroline N-oxide (DMPO) as the trapping reagent. As shown in Fig. 5, six obvious signals attributing to $O_2^{\bullet-}$ were observed in our Fe-ZnS/NC 650/methanol/air system, while the signal was hardly detected in NC 650, confirming the role of Fe-ZnS/NC 650 in O_2 activation to $O_2^{\bullet-}$ during β-O-4 oxidative cleavage [19].

3.3. Exploration for C-C/C-O cleavage sites on Fe-ZnS/NC 650

To probe the active center for C-C/C-O cleavage in β-O-4 over Fe-ZnS/NC 650, we analyzed the β-O-4 (1) activation energy on ZnS and FeS sites using DFT calculation. Fig. 6**A** showed the bond lengths of C_α-C_β (1.220 Å) and C_α =O (1.473 Å) of the free β-O-4 (1) compound and Fig. 6**B** displayed the bond lengths of the adsorbed β-O-4 (1) on Fe-ZnS/NC 650. It showed that both the bond lengths of C_α-C_β and C_α =O increased on ZnS sites and FeS sites, while the β-O-4 (1) adsorption energies were relatively lower on ZnS sites of − 1.744 eV comparing with the − 1.423 eV on FeS sites. The above results implied that β-O-4 (1) tended to be adsorbed by ZnS sites. Afterwards, the carbonyl group in β-O-4 (1) was more likely polarized by ZnS site and made C_β-H acidification, contributing the formation of hydroperoxide intermediate due to the attack by $O_2^{\bullet-}$ (Fig. 6**C**). The formed hydroperoxide could be converted into *α*-diketone (Fig. 6**D**) via Kornblum-DelaMare rearrangement [42]. Followingly, the *α*-diketone intermediate was then converted into phenyl formate **(f)** and methyl benzoate **(b)** through C-C cleavage (**Route B**, Fig. 7**B**), or phenol **(a)** and phenylglyoxal **(e)** through C-O cleavage (**Route A,** Fig. 7**B**). The existence of phenylglyoxal **(e)** was proved by lowering down the reaction condition to 80 °C for 2 h during β-O-4 (1) oxidation (Fig. S6)**.**

The formed phenylglyoxal **(e)** and phenyl formate **(f)** intermediates could be further transformed, which has been confirmed by a serious of experiments. As shown in Scheme 2**i,** phenylglyoxal **(e)** could be fully converted to methyl benzoate **(b)** and methyl benzoylformate **(c)** under the Fe-ZnS/NC 650/methanol/air system; meanwhile, the formed methyl benzoylformate **(c)** could be also converted to methyl benzoate **(b)** by our catalytic system despite of the low conversion and yield (Scheme 2**ii).** Another important possible intermediate, phenyl formate **(f)**, was also fully converted to phenol **(a)** under our catalytic system (Scheme 2**iii**).

Based on the experimental results and DFT calculation, we proposed that the excellent oxidative activity of Fe-ZnS/NC 650 in β-O-4 (1) cleavage originated from the synergistic function of FeS sites and ZnS sites. As shown in Fig. 7**A**, O_2 would be firstly activated into superoxide radical ($O_2^{\bullet-}$) by FeS sites (**II**), and β-O-4 (1) will mostly adsorb on ZnS

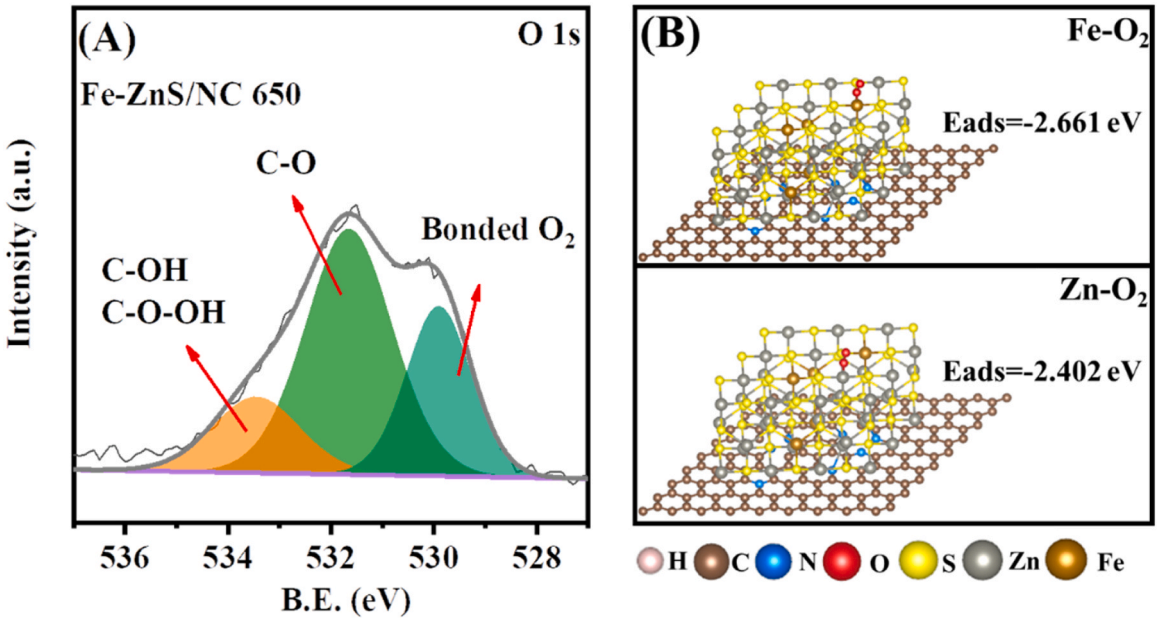

Fig. 4. (A) O 1 s XPS spectra of Fe-ZnS/NC 650**, (B)** Fe-ZnS/NC model with optimized geometry by DFT calculation: O_2 activation on FeS sites (top) or ZnS sites (bottom).

Table 3
Catalytic oxidation of β-O-4 (1) with different scavengers by Fe-ZnS/NC 650.

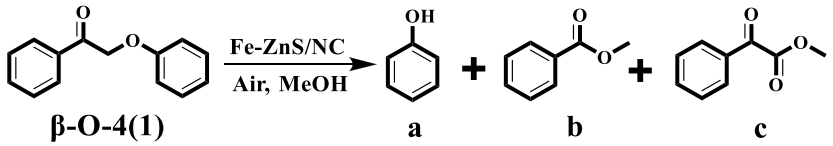

Label	Conv. (%)
None quencher	99.0
Isopropanol (•OH)	99.0
Furfuryl alcohol ($^1O_2$)	92.9
1,4-Benzoquinone (O_2•)	7.0

Reaction conditions: substrate (20 mg), catalyst (20 mg), methanol (20 mL), air (1 MPa), 120 °C, 2 h. 4 equiv. quencher.

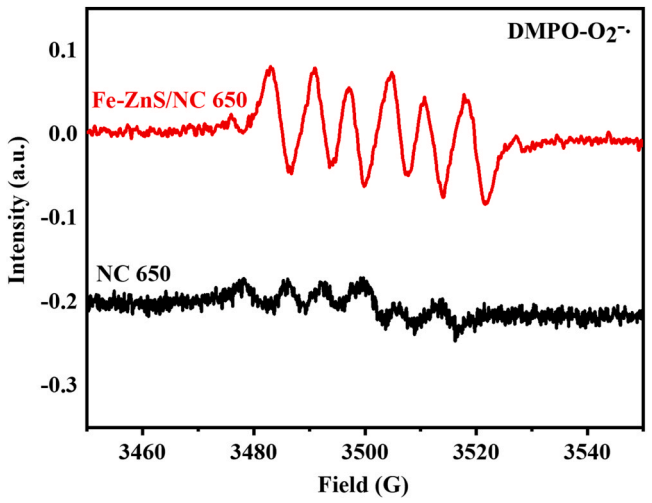

Fig. 5. The EPR spectra of the DMPO-O_2^-• recorded over Fe-ZnS/NC 650 and NC 650.

sites that would polarize the carbonyl group and acidify the C_β-H. Subsequently, the O_2^-• would then interact with the acidified C_β-H in β-O-4 (1) adsorbed on ZnS sites (**III**), which triggered the oxidation reaction of C_β-H into hydroperoxide intermediate (**IV**). The formed hydroperoxide intermediate could be converted further into diketone (**V**) which was then depolymerized through two main routes. For **Route A**, the diketone intermediate (**V**) would be directly cleaved into phenol (**a**) and phenylglyoxal (**e**) through C-O cleavage. Afterwards, phenylglyoxal (**e**) was converted into methyl benzoate (**b**), and methyl benzoylformate (**c**) over Fe-ZnS/NC 650 that has been confirmed in **Scheme 2i.** For **Route B**, the diketone intermediate (**V**) was cleaved through C-C cleavage, providing phenyl formate (**f**) and methyl benzoate (**b**), where phenyl formate (**f**) would be further converted in to phenol (**a**) on Fe-ZnS/NC 650 which has been proved in **Scheme 2iii**. Therefore, the excellent catalytic activity of Fe-ZnS/NC 650 came from the dual reaction sites of FeS and ZnS sites, which reduced the migration distance of superoxide radicals that could only exist for a short time compared with that on solely FeS/NC or ZnS/NC, thus improving the catalytic oxidative performance for β-O-4 (1) depolymerization. Moreover, the activation energies required for C-C and C-O cleavage and product formation were calculated. As shown in Fig. 7**B**, the activation energy for C-C cleavage (0.67 eV, **Route B**) was higher than that for C-O cleavage (0.54 eV, **Route A**), along with the relatively lower monomers formation energies (−0.43 eV, **Route A**) than that of 0.41 eV for **Route B**. The above information indicated that **Route A** was more likely to occur in our system than **Route B**.

3.4. Oxidative depolymerization of lignin

Our previous study reported the controlled oxidation of lignin linkages (e.g., β-O-4 or β-β) to specific degree using DDQ as the oxidant [31]. In the present work, we employed the medium oxidized beech lignin (labeled as lignin^{OX}) by 1.33 wt% equiv. DDQ, and then Fe-ZnS/NC 650 was applied to the depolymerization of beech lignin^{OX} (Table 4). The products were analyzed by mass spectrometry and quantified by internal standard method by GC-FID (Fig. S8 **& S9**). Similar to the products obtained in model compounds, the beech lignin^{OX} was mostly converted to carbonyl-containing monomers with up to 92% selectivity (e.g, **b'**-methyl vanillate and **b''**-methyl syringate) among the total detected monomers in the presence of Fe-ZnS/NC 650. The monomer yields showed upward trend when increasing reaction time (entry 1–3, i.e., the total yields increased from 9.60 wt% to 11.81 wt% when prolonging the reaction time from 2 to 6 h, together with the yield of **b'** (or **b"**) increasing from 1.15 wt% (5.89 wt%) to 1.39 wt% (7.41 wt%). The total monomer yields obtained here were comparable, at least not worse, than the values reported by other researchers, especially under alkaline-free condition in air (Table S5). No significant increase of monomers yield was observed when further increasing the reaction time to 8 or 10 h, and hence 6 h was used for the followed test.

The total monomers yield lowered down to 7.48 wt% in the absence of Fe-ZnS/NC 650 (entry 6), which demonstrated the effectiveness of Fe-ZnS/NC 650 on real lignin degradation. The catalytic activity also decreased when the reaction was carried out under N_2, with the total monomer yields dropping to 7.06 wt% (entry 7), indicating that the O_2^-• produced from O_2 activation was highly required for lignin oxidative depolymerization. It should note that the yield of acetosyringone (**g'**) significantly increased to 2.85 wt% under 1 MPa N_2 comparing with the 0.63 wt% under 1 MPa air (entry 3), suggesting that the existence of O_2 inhibited the formation of acetosyringone (**g'**). Especially, the yield of acetosyringone (**g'**) was even higher than methyl syringate (**b''**, 2.23 wt %) which was detected as the main products under air condition, and we hence assumed that acetosyringone (**g'**) might be formed in parallel through different route as methyl syringate (**b''**) did, which will be detailly discussed in Scheme 3.

2D HSQC NMR was performed to analyze the evolution of typical linkages in beech lignin^{OX} (Fig. 8). As shown in Fig. 8**A**, the beech lignin^{OX} possessed mainly oxidized β-O-4 ketone linkages (**A''β** and **A'β**) at the range of 5–6/80–85 ppm (H^1/C^{13}), where **A''β** stranded for the oxidized β-O-4 with an adjacent oxidized β-O-4 and **A'β** represented oxidized β-O-4 with an adjacent unoxidized β-O-4 [31]. Meanwhile, the unoxidized β-O-4 (**Aβ**) could be also detected at around 4.7/72.5 ppm (H^1/C^{13}) due to the low oxidation degree when using 1.33 wt. equiv. DDQ, which was in accordance with our previous reports [31]. With the catalytic function by our developed Fe-ZnS/NC 650/methanol/air system, the β-O-4 linkages including the oxidized linkages (**A''β** and **A'β**) and unoxidized ones (**Aβ**) were seldomly detected, indicating that most of the β-O-4 linkages were cleaved over Fe-ZnS/NC 650. More importantly, large quantity of new signals at around 3.5–4.0/50–55 ppm

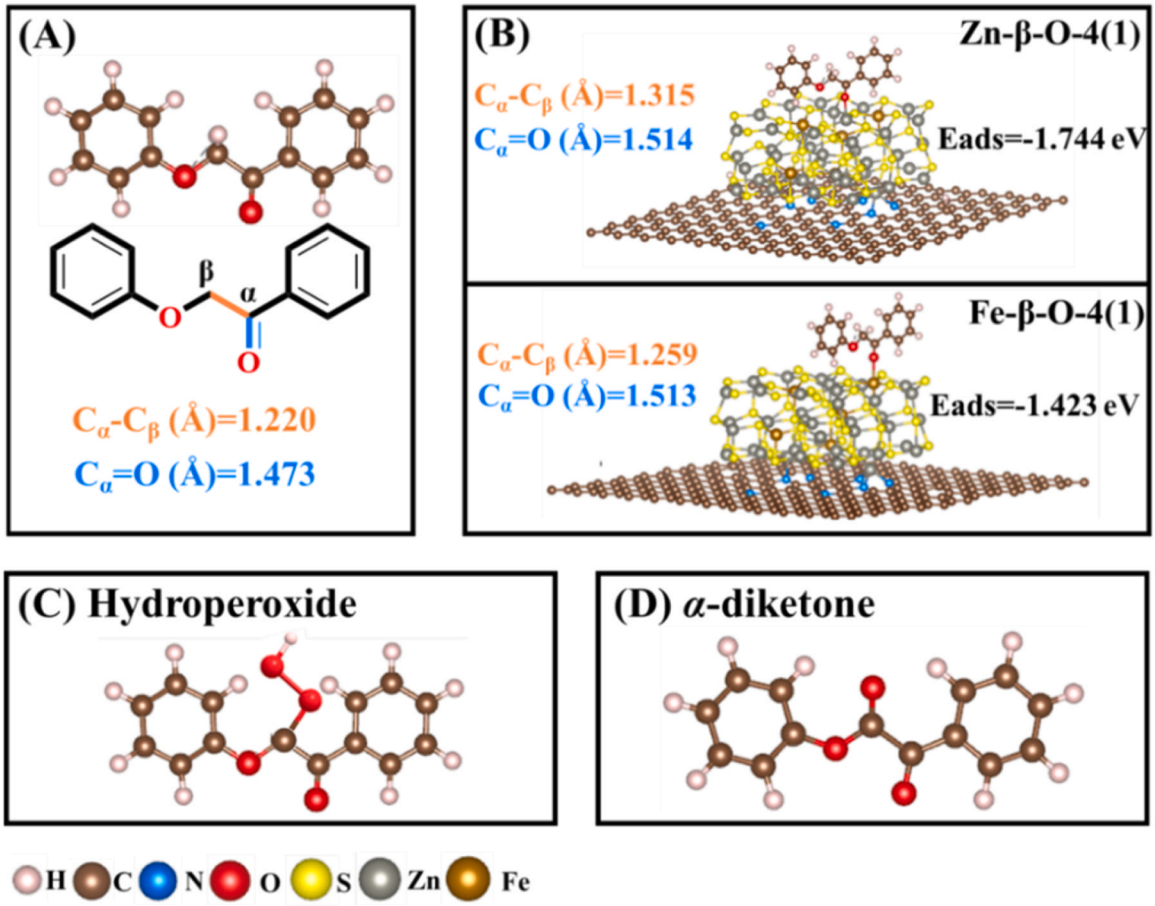

Fig. 6. **(A)** The bond length of C_{α}-C_{β} or C_{α} =O in free β-O-4 (1) compound; **(B)** The optimized geometry of β-O-4 (1) adsorbed on Fe-ZnS/NC by DFT calculation: the bond length of C_{α}-C_{β} or C_{α} =O of the activated β-O-4 (1) and the adsorption energy of β-O-4 (1) on ZnS or FeS; the model of **(C)** hydroperoxide and **(D)** a-diketone.

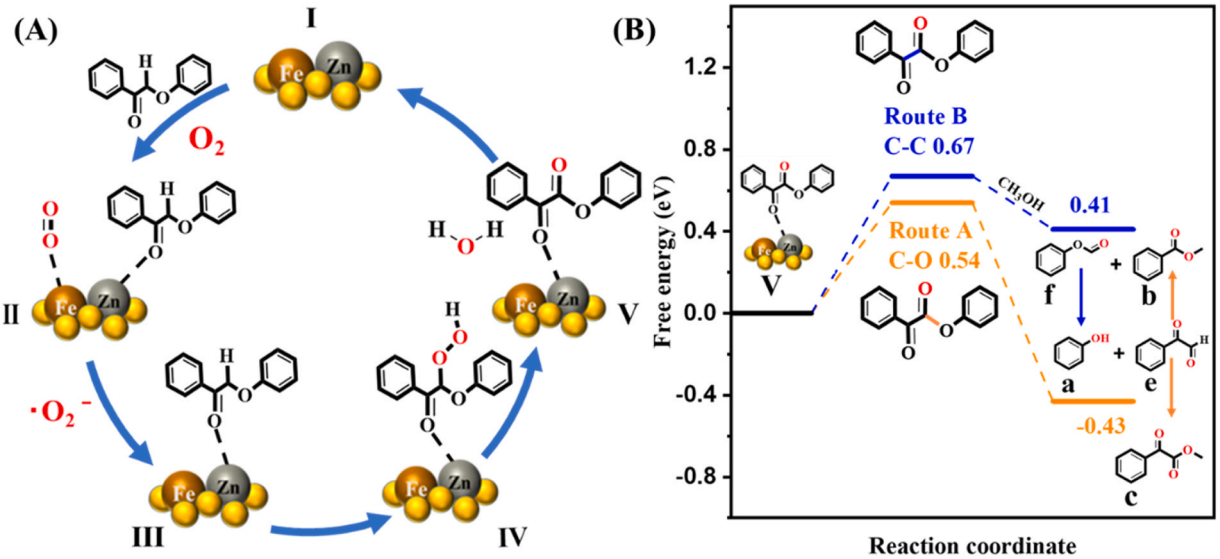

Fig. 7. **(A)** Proposed reaction mechanism of β-O-4 on Fe-ZnS/NC 650; **(B)** activation energy required for β-O-4 (1) conversion.

(H^1/C^{13}) (green circle, Fig. 8**B**) were observed. The new occurred signals were attributed to the methoxyl connected with the linkages [43] of the depolymerized products (e.g., **b'**-methyl vanillate and **b''**-methyl syringate, Table 4). The above results further confirmed the excellent oxidation activity of Fe-ZnS/NC 650 for C-O/C-C cleavage in lignin depolymerization.

Based on all the above discussion, a possible oxidative pathway for beech $lignin^{OX}$ depolymerization over Fe-ZnS/NC 650 was proposed (Scheme 3). Similar to model compound, O_2 would be also firstly activated by FeS to form superoxide radicals, and the superoxide radicals then reacted with ZnS-activated C_{β}-H to form hydroperoxide (**B**). The formed hydroperoxide could be converted into diketone (**C**) which was

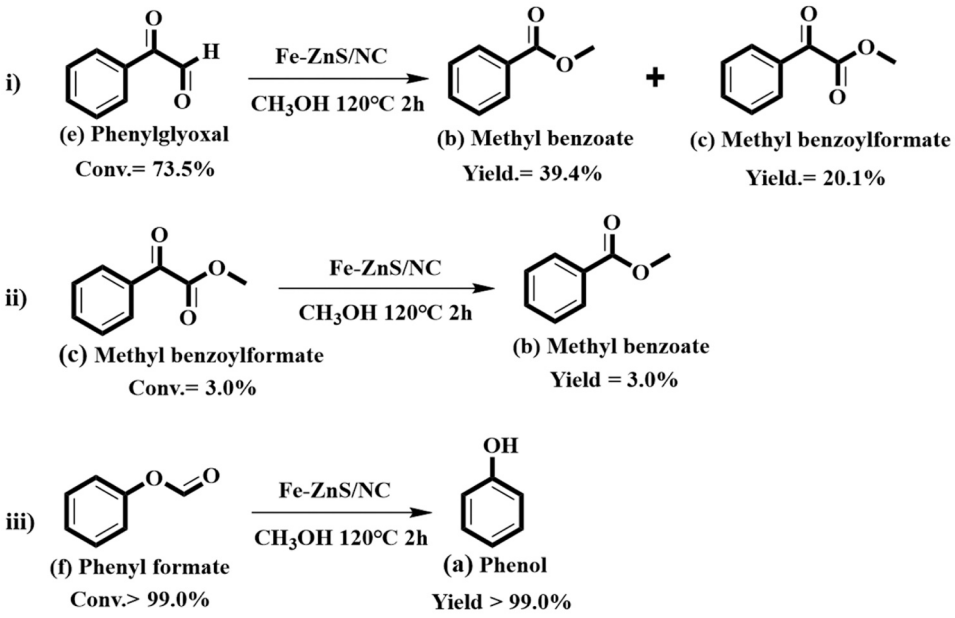

Scheme 2. Exploration of possible reaction paths of β-O-4 (1) over Fe-ZnS/NC 650 methanol/air system.

Table 4
The catalytic oxidative cleavage of beech lignin under various conditions.

Entry	Time (h)	b'	b"	d'	d"	g'	h'	Total yield (wt %)	Carbonyl-containing monomers selectivity (%)
1	2	1.15	5.89	0.58	0.76	0.42	0.80	9.60	92
2	4	1.13	6.75	0.57	0.86	0.50	0.86	10.67	92
3	6	1.39	7.41	0.57	0.82	0.63	0.92	11.81	92
4	8	1.43	7.52	0.64	0.94	0.55	0.85	11.72	92
5	10	1.56	6.85	0.44	0.84	0.74	1.14	11.57	90
6[a]	6	1.10	5.18	0.48	-	0.32	0.43	7.48	95
7[b]	6	0.43	2.23	0.39	0.50	2.85	0.66	7.06	90

Reaction condition: oxidized dioxasolv beech lignin (lignin^{OX}, 100 mg), Fe-ZnS/NC 650 (50 mg), methanol (20 mL), 200 °C, 1 MPa air, 2–10 h.
a: Catalyst-free.
b: 1 MPa N_2.

then cleaved through two main routes. For **C-C bond** cleavage path, diketone (**C**) would be cleaved into esterification products (**b'** or **b"**) with the participance of methanol, or syringaldehyde (**h'**) without methanol [44]. For the **C-O bond** cleavage path, diketone (**C**) could be converted to aromatic alcohols **d'** or **d"**. It should note that initial oxidized β-O-4 (**A**) could be also converted into acetosyringone (**g'**) directly under O_2-free condition, in which case acetosyringone (**g'**) would be the main product which has been proved by the result in Table 4.

4. Conclusion

In conclusion, we developed H_2S-free self S-doping Fe-ZnS/NC bimetallic catalyst using waste lignin as carbon/sulfur precursors, and the Fe-ZnS/NC 650 showed excellent aerobic oxidative activity (> 99% conversion and > 80% monomers yield) for C-O/C-C cleavage in a serious of β-O-4 model compounds under mild condition (120 °C, 2 h, acid/base free), exceeding the catalysts with only FeS or ZnS sites. Control experiments and density functional theory (DFT) calculations disclosed the dual function of FeS sites and ZnS sites in lignin oxidative cleavage, on which the FeS sites contributed to the O_2 activation into O_2^{-}• that would then attack the acidified C_β-H of the β-O-4 adsorbed on ZnS into hydroperoxide intermediate. The hydroperoxide intermediate would then transform into diketone followed by its subsequent C-C/C-O cleavage into aromatic monomers. The co-existence of FeS and ZnS dual sites reduced the migration distance of the O_2^{-}• to the polarized β-O-4 linkage, thus accelerating C-O/C-C oxidative cleavage. The good oxidative activity of Fe-ZnS/NC 650 could also be feasible for the depolymerization of oxidized lignin, where the β-O-4 linkages was effectively converted into aromatic monomers (11.81 wt%) with 92% of carbonyl-containing products selectivity through 2D HSQC NMR analysis and depolymerization results. The present work provided a promising strategy to obtain carbonyl-containing aromatics with high selectivity by lignin oxidation using H_2S-free and self S-doped FeZn sulfide bimetallic catalyst under alkaline-free condition.

CRediT authorship contribution statement

Zhao Chen: Methodology, Validation, Investigation, Writing – original draft. **Qiqi Yin & Tian Sun:** Formal analysis, Data curation. **Yuxuan Liu & Gengbo Ren:** Investigation, Methodology. **Haiwei Guo & Changzhi Li:** Writing – review & editing, Supervision, Funding acquisition.

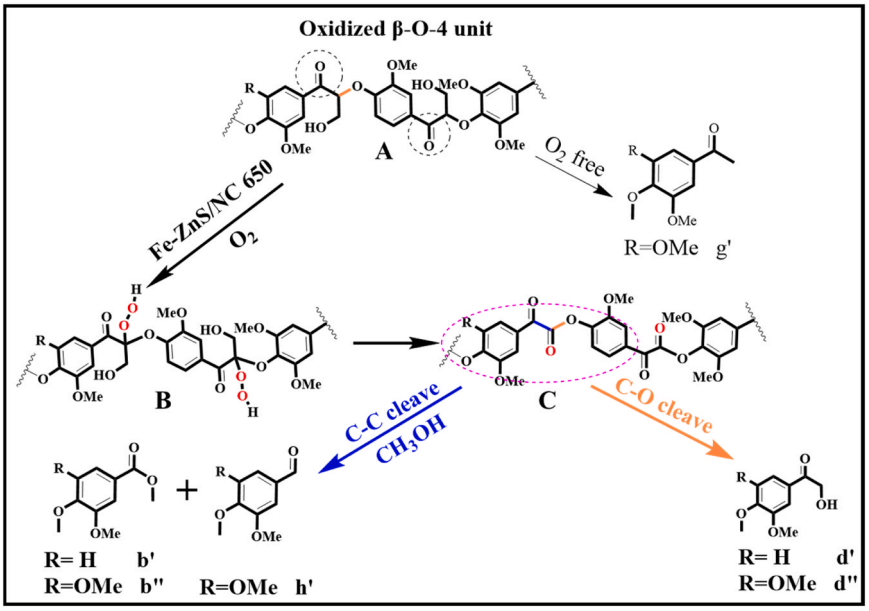

Scheme 3. Proposed depolymerization route of beech lignin^{OX} over Fe-ZnS/NC 650/methanol/air system.

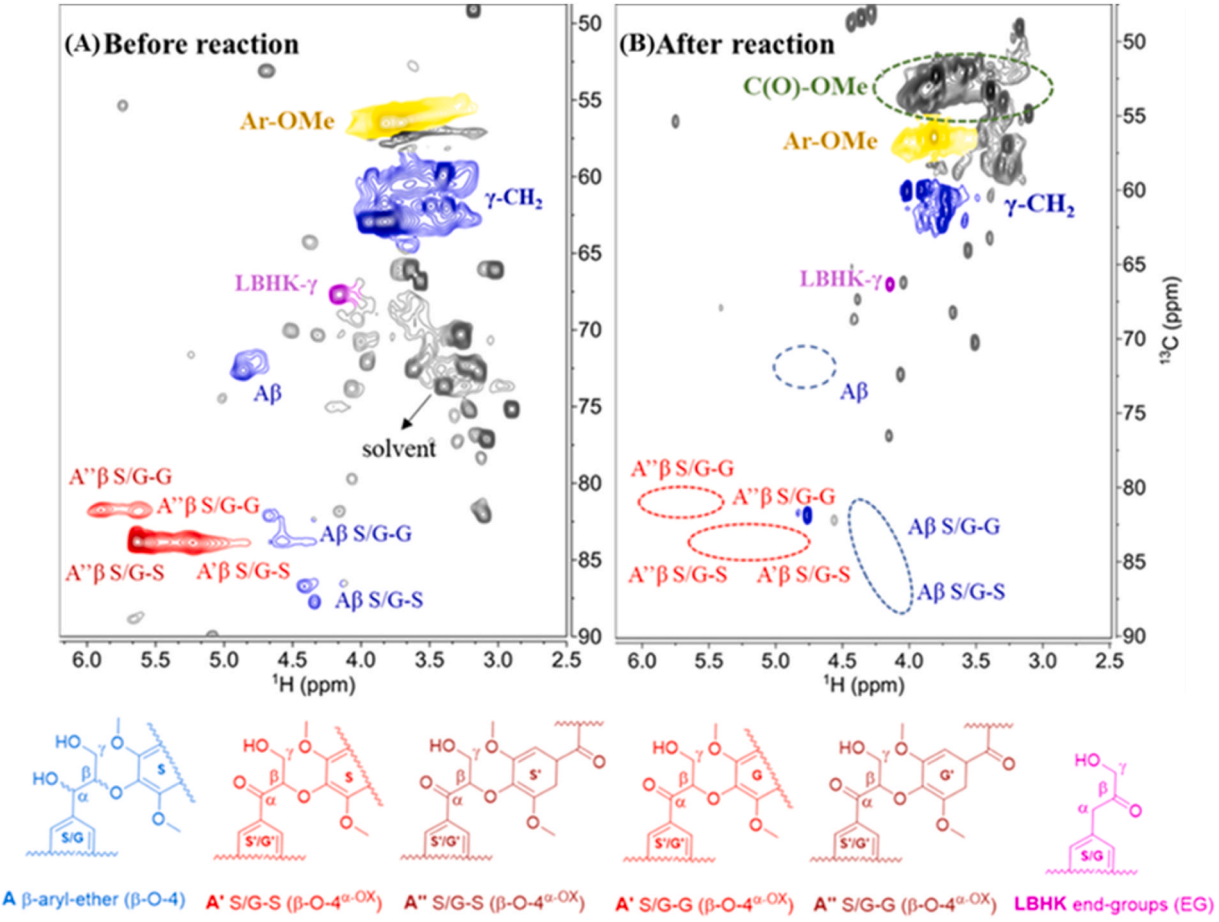

Fig. 8. 2D NMR spectra of lignin^{OX} (**A**) before reaction and (**B**) after reaction. Different colors of cross peaks represented different linkages in lignin. Reaction conditions: beech lignin^{OX} (100 mg), Fe-ZnS/NC 650 (50 mg), methanol (20 mL), 200 °C, 1 MPa air, 10 h.

Declaration of Competing Interest

The authors declare that they have no known competing financial interests or personal relationships that could have appeared to influence the work reported in this paper.

Data Availability

Data will be made available on request.

Acknowledgment

This work was supported by the National Key R&D Program of China (2019YFC1905300) and National Natural Science Foundation of China (No. 22108058, 22311530058).

Appendix A. Supporting information

Supplementary data associated with this article can be found in the online version at doi:10.1016/j.apcatb.2023.123129.

References

[1] X. Yue, L. Zhang, L. Sun, S. Gao, W. Gao, X. Cheng, N. Shang, Y. Gao, C. Wang, Highly efficient hydrodeoxygenation of lignin-derivatives over Ni-based catalyst, Appl. Catal. B 293 (2021), 120243.
[2] X. Dou, W. Li, C. Zhu, X. Jiang, Catalytic waste kraft lignin hydrodeoxygenation to liquid fuels over a hollow Ni-Fe catalyst, Appl. Catal. B 287 (2021), 119975.
[3] W. Deng, Y. Feng, J. Fu, H. Guo, Y. Guo, B. Han, Z. Jiang, L. Kong, C. Li, H. Liu, P.T. T. Nguyen, P. Ren, F. Wang, S. Wang, Y. Wang, Y. Wang, S. Wong, K. Yan, N. Yan, X. Yang, Y. Zhang, Z. Zhang, X. Zeng, H. Zhou, Catalytic conversion of lignocellulosic biomass into chemicals and fuels, Green Energy Environ. 8 (2023) 10–114.
[4] Y. Liao, S.F. Koelewijn, G.V.D. Bossche, J.V. Aelst, S.V.D. Bosch, T. Renders, K. Navare, T. Nicolaï, K.V. Aelst, M. Maesen, H. Matsushima, J.M. Thevelein, K. V. Acker, B. Lagrain, D. Verboekend, B.F. Sels, A sustainable wood biorefinery for low-carbon foot-print chemicals production, Science 367 (2020) 1385–1390.
[5] L. Zhang, N. Shang, S. Gao, J. Wang, T. Meng, C. Du, T. Shen, J. Huang, Q. Wu, H. Wang, Y. Qiao, C. Wang, Y. Gao, Z. Wang, Atomically dispersed co catalyst for efficient hydrodeoxygenation of lignin-derived species and hydrogenation of nitroaromatics, ACS Catal. 10 (2020) 8672–8682.
[6] K. Lee, Y. Jing, Y. Wang, N. Yan, A unified view on catalytic conversion of biomass and waste plastics, Nat. Rev. Chem. 6 (2022) 635–652.
[7] R. Behling, S. Valange, G. Chatel, Heterogeneous catalytic oxidation for lignin valorization into valuable chemicals: what results? What limitations? What trends? Green. Chem. 18 (2016) 1839–1854.
[8] C. Liu, S. Wu, H. Zhang, R. Xiao, Catalytic oxidation of lignin to valuable biomass-based platform chemicals: a review, Fuel Process. Technol. 191 (2019) 181–201.
[9] M. Wang, L. Li, J. Lu, H. Li, X. Zhang, H. Liu, N. Luo, F. Wang, Acid promoted C-C bond oxidative cleavage of β-O-4 and β-1 lignin models to esters over a copper catalyst, Green Chem. 19 (2017) 702–706.
[10] Y. Hu, L. Yan, X. Zhao, C. Wang, S. Li, X. Zhang, L. Ma, Q. Zhang, Mild selective oxidative cleavage of lignin C-C bonds over a copper catalyst in water, Green Chem. 23 (2021) 7030–7040.
[11] C. Yang, S. Maldonado, C.R.J. Stephenson, Electrocatalytic lignin oxidation, ACS Catal. 11 (2021) 10104–10114.
[12] S. Liu, A.P. vanMuyden, L. Bai, X. Cui, Z. Fei, X. Li, X. Hu, P.P.J. Dyson, Metal-sulfide catalysts derived from lignosulfonate and their efficient use in hydrogenolysis, ChemSusChem 12 (2019) 3271–3277.
[13] L. Wu, P. Guo, X. Wang, H. Li, X. Zhang, K. Chen, P. Zhou, The synergy of sulfur vacancies and heterostructure on CoS-FeS nanosheets for boosting the peroxymonosulfate activation, Chem. Eng. J. 446 (2022), 136759.
[14] R. Gusain, N. Kumar, F. Opoku, P.P. Govender, S.S. Ray, MoS_2 nanosheet/ZnS composites for the visible-light-assisted photocatalytic degradation of oxytetracycline, ACS Appl. Nano Mater. 4 (2021) 4721–4734.
[15] J. Lin, X. Wu, S. Xie, L. Chen, Q. Zhang, W. Deng, Y. Wang, Visible-light-driven cleavage of C-O linkage for lignin valorization to functionalized aromatics, ChemSusChem 12 (2019) 5023–5031.
[16] Z. Fang, F. Li, M. Wang, F. Li, X. Wu, K. Fan, Q. Tang, L. Sun, P. Zhang, Selective electrocatalytic upgrading of lignin to aryl aldehydes and carboxylic acids over dodecyl sulfate-intercalated CoS nanocones, Appl. Catal. B 323 (2023), 122149.
[17] G. Han, T. Yan, W. Zhang, Y. Zhang, D.Y. Lee, Z. Cao, Y. Sun, Highly selective photocatalytic valorization of lignin model compounds using ultrathin metal/CdS, ACS Catal. 9 (2019) 11314–11349.
[18] J. Qin, B. Han, X. Liu, W. Dai, Y. Wang, H. Luo, X. Lu, J. Nie, C. Xian, Z. Zhang, An enzyme-mimic single Fe-N_3 atom catalyst for the oxidative synthesis of nitriles via C-C bond cleavage strategy, Sci. Adv. 8 (2022) 1267.
[19] C. Xie, L. Lin, L. Huang, Z. Wang, Z. Jiang, Z. Zhang, B. Han, Zn-N_x sites on N-doped carbon for aerobic oxidative cleavage and esterification of C(CO)-C bonds, Nat. Commun. 12 (2021) 4823.
[20] X. Li, X. Huang, S. Xi, S. Miao, J. Ding, W. Cai, S. Liu, X. Yang, H. Yang, J. Gao, J. Wang, Y. Huang, T. Zhang, B. Liu, Single cobalt atoms anchored on porous N-doped graphene with dual reaction sites for efficient fenton-like catalysis, J. Am. Chem. Soc. 140 (2018) 12469–12475.
[21] E.A. Moges, C. Chang, W. Huang, K. Lakshmanan, Y.A. Awoke, C. Pao, M. Tsai, W. Su, B.J. Hwang, Sustainable synthesis of dual single-atom catalyst of Pd-N_4/Cu-N_4 for partial oxidation of ethylene glycol, Adv. Funct. Mater. 32 (2022) 3271–3277.
[22] T. Gao, C. Lu, C. Hu, L. Lyu, H_2O_2 inducing dissolved oxygen activation and electron donation of pollutants over Fe-ZnS quantum dots through surface electron-poor/rich microregion construction for water treatment, J. Hazard. Mater. 420 (2021), 126579.
[23] K. Wu, W. Wang, H. Guo, Y. Yang, Y. Huang, W. Li, Ch Li, Engineering Co nanoparticles supported on defect MoS_{2-x} for mild deoxygenation of lignin-derived phenols to arenes, ACS Energy Lett. 5 (2020) 1330–1336.
[24] N. Luo, T. Montini, J. Zhang, P. Fornasiero, E. Fonda, T. Hou, W. Nie, J. Lu, J. Liu, M. Heggen, L. Lin, C. Ma, M. Wang, F. Fan, S. Jin, F. Wang, Visible-light-driven coproduction of diesel precursors and hydrogen from lignocellulose-derived methylfurans, Nat. Energy 4 (2019) 575–584.
[25] F. Jamal, A. Rafique, S. Moeen, J. Haider, W. Nabgan, A. Haider, M. Imran, G. Nazir, M. Alhassan, M. Ikram, Q. Khan, G. Ali, M. Khan, W. Ahmad, M. Maqbool, Review of metal sulfide nanostructures and their applications, ACS Appl. Nano Mater. 6 (2023) 7077–7106.
[26] H. Zhou, S. Hong, H. Zhang, Y. Chen, H. Xu, X. Wang, Z. Jiang, S. Chen, Y. Liu, Toward biomass-based single-atom catalysts and plastics: Highly active single-atom Co on N-doped carbon for oxidative esterification of primary alcohols, Appl. Catal. B 256 (2019), 117767.
[27] Y. Qi, J. Li, Y. Zhang, Q. Cao, Y. Si, Z. Wu, M. Akram, X. Xu, Novel lignin-based single atom catalysts as peroxymonosulfate activator for pollutants degradation: Role of single cobalt and electron transfer pathway, Appl. Catal. B 286 (2021), 119910.
[28] C. Zhang, H. Li, J. Lu, X. Zhang, E. MacArthur K, M. Heggen, F. Wang, Promoting lignin depolymerization and restraining the condensation via an oxidation-hydrogenation strategy, ACS Catal. 7 (2017) 3419–3429.
[29] T. Tana, Z. Zhang, J. Beltramini, H. Zhu, K. Ostrikov, J. Bartley, W. Doherty, Valorization of native sugarcane bagasse lignin to bio-aromatic esters/monomers via a one pot oxidation-hydrogenation process, Green. Chem. 21 (2019) 861–873.
[30] H. Guo, D.M. Miles-Barrett, B. Zhang, A. Wang, T. Zhang, N.J. Westwood, C. Li, Is oxidation-reduction a real robust strategy for lignin conversion? A comparative study on lignin and model compounds, Green Chem. 21 (2019) 803–811.
[31] H. Guo, D.M. Miles-Barrett, A.R. Neal, T. Zhang, C. Li, J. Westwood N, Unravelling the enigma of $lignin^{OX}$: can the oxidation of lignin be controlled? Chem. Sci. 9 (2018) 702–711.
[32] K. Chen, C. Song, Z. Huang, L. Rao, X. Jin, G. Liu, F. He, Q. Huang, Thermally regenerable FeS/N-doped biochar catalyzed peroxydisulfate oxidative destruction of aqueous triclosan, Chem. Eng. J. 462 (2023), 142152.
[33] X. Hao, Y. Wang, J. Zhou, Z. Cui, Y. Wang, Z. Zou, Zinc vacancy-promoted photocatalytic activity and photostability of ZnS for efficient visible-light-driven hydrogen evolution, Appl. Catal. B 221 (2018) 302–311.
[34] P. Li, H. Wang, W. Fan, M. Huang, J. Shi, Z. Shi, S. Liu, Salt assisted fabrication of lignin-derived Fe, N, P, S codoped porous carbon as trifunctional catalyst for Zn-air batteries and water-splitting devices, Chem. Eng. J. 421 (2021), 129704.
[35] Li. Yu, L. Yang, X. Li, T. Miki, T. Nagasaka, A composite adsorbent of ZnS nanoclusters grown in zeolite NaA synthesized from fly ash with a high mercury ion removal efficiency in solution, J. Hazard. Mater. 411 (2021), 125044.
[36] D. Yang, D. Yadav, I. Jeon, J. Seo, S. Jeong, C. Cho, Enhanced high-rate capability and long cycle stability of FeS@NCG nanofibers for sodium-ion battery anodes, ACS Appl. Mater. Interfaces 14 (2022) 44303–44316.
[37] J. Ge, J. Zheng, J. Zhang, S. Jiang, L. Zhang, H. Wan, L. Wang, W. Ma, Z. Zhou, R. Ma, Controllable atomic defect engineering in layered $NixFe_{1-x}(OH)_2$ nanosheets for electrochemical overall water splitting, J. Mater. Chem. A 9 (2021) 14432–14443.
[38] H. Guo, B. Zhang, C. Li, C. Peng, T. Dai, H. Xie, A. Wang, T. Zhang, Tungsten carbide: a remarkably efficient catalyst for the selective cleavage of lignin C-O bonds, ChemSusChem 9 (2016) 3220–3229.
[39] Z. Cai, J. Long, Y. Li, L. Ye, B. Yin, L.J. France, J. Dong, L. Zheng, H. He, S. Liu, S.C. E. Tsang, X. Li, Selective production of diethyl maleate via oxidative cleavage of lignin aromatic unit, Chem 5 (2019) 2365–2377.
[40] L. Li, J. Kong, H. Zhang, S. Liu, Q. Zeng, Y. Zhang, H. Ma, H. He, J. Long, X. Li, Selective aerobic oxidative cleavage of lignin C-C bonds over novel hierarchical Ce-Cu/MFI nanosheets, Appl. Catal. B 279 (2020), 119343.
[41] S. Shang, P. Chen, L. Wang, Y. Lv, W. Li, Metal-free nitrogen-and boron-codoped mesoporous carbons for primary amides synthesis from primary alcohols via direct oxidative dehydrogenation, ACS Catal. 8 (2018) 9936–9944.
[42] J.D. Grayson, B.M. Partridge, Mild Cu-catalyzed oxidation of benzylic boronic esters to ketones, ACS Catal. 9 (2019) 4296–4301.
[43] W. Xu, X. Li, J. Shi, Oxidative depolymerization of cellulolytic enzyme lignin over silicotungvanadium polyoxometalates, Polymers 11 (2019) 564.
[44] P. Guo, S. Liao, S. Wang, J. Shi, X. Tong, Highly efficient and selectivity-controllable aerobic oxidative cleavage of C-C bond over heterogeneous Fe-based catalysts, J. Catal. 395 (2021) 399–403.